Valparaiso University
ValpoScholar

12-1-2016

Observational Confirmation of a Link between Common Envelope Binary Interaction and Planetary Nebula Shaping

Todd Hillwig
Valparaiso University, todd.hillwig@valpo.edu

David Jones
Instituto de Astrofísica de Canarias

Orsola De Marco
Universidad de La Laguna

Howard E. Bond
Pennsylvania State University

Steve Margheim

See next page for additional authors

Follow this and additional works at: http://scholar.valpo.edu/phys_astro_fac_pub

Authors

Todd Hillwig, David Jones, Orsola De Marco, Howard E. Bond, Steve Margheim, and David Frew

OBSERVATIONAL CONFIRMATION OF A LINK BETWEEN COMMON ENVELOPE BINARY INTERACTION AND PLANETARY NEBULA SHAPING

Todd C. Hillwig[1,9], David Jones[2,3], Orsola De Marco[4], Howard E. Bond[5,6,9], Steve Margheim[7], and David Frew[8]

[1] Department of Physics and Astronomy, Valparaiso University, Valparaiso, IN 46383, USA; Todd.Hillwig@valpo.edu
[2] Instituto de Astrofísica de Canarias, E-38205 La Laguna, Tenerife, Spain
[3] Departamento de Astrofísica, Universidad de La Laguna, E-38206 La Laguna, Tenerife, Spain
[4] Department of Physics and Astronomy, Macquarie University, Sydney, NSW 2109, Australia
[5] Department of Astronomy & Astrophysics, Pennsylvania State University, University Park, PA 16802, USA
[6] Space Telescope Science Institute, 3700 San Martin Drive, Baltimore, MD 21218, USA
[7] Gemini Observatory, Southern Operations Center, Casilla 603, La Serena, Chile
[8] Department of Physics, The University of Hong Kong, Pokfulam Road, Hong Kong

ABSTRACT

A current issue in the study of planetary nebulae with close binary central stars (CSs) is the extent to which the binaries affect the shaping of the nebulae. Recent studies have begun to show a high coincidence rate between nebulae with large-scale axial or point symmetries and close binary stars. In addition, combined binary-star and spatiokinematic modeling of the nebulae have demonstrated that all of the systems studied to date appear to have their central binary axis aligned with the primary axis of the nebula. Here we add two more systems to the list, the CSs and nebulae of NGC 6337 and Sp 1. We show both systems to be low inclination, with their binary axis nearly aligned with our line of sight. Their inclinations match published values for the inclinations of their surrounding nebulae. Including these two systems with the existing sample statistically demonstrates a direct link between the central binary and the nebular morphology. In addition to the systems' inclinations we give ranges for other orbital parameters from binary modeling, including updated orbital periods for the binary CSs of NGC 6337 and Sp 1.

Key words: binaries: close – planetary nebulae: general – planetary nebulae: individual (NGC 6337, Sp 1)

Supporting material: machine-readable tables

1. INTRODUCTION

The shaping of planetary nebulae (PNe) has been a matter of interest for some time with the problem being approached from a number of different but complementary methods (Kwitter et al. 2014). One approach has been to identify binary central stars (CSs) where the companions are close enough to have interacted in the past and determine whether the interaction might have produced the observed morphologies. Since most known binary CSs are post-common-envelope (CE) binaries (for a recent review of the CE binary interaction, see Ivanova et al. 2013), it is the CE interaction that has been primarily under scrutiny.

Searches for close binary central stars of planetary nebulae (CSPNe) have been successful in discovering these systems, showing that approximately 10%–20% of all CSPNe appear to have a binary companion with an orbital period of less than a few days (Bond 2000; De Marco 2009; Miszalski et al. 2009a). Many of those systems were discovered through photometric variability, and while most are likely to be real binaries, additional confirmation is necessary for some of them (e.g., Kn 61; De Marco et al. 2015). Along with studies confirming the binarity of several of these systems (e.g., Shimanskii et al. 2008; Hillwig et al. 2015, 2016), discoveries of additional close binary CSPNe are helping us to better understand the nature of these systems. In addition, studies of the CS can be linked to kinematic studies of the nebulae to determine whether a causal link exists between the interaction and the nebular morphology and kinematics.

Surprisingly, while there are several suggestions that the CE interaction is the cause for the shape of post-CE PNe (Morris 1981; Bond & Livio 1990; Zijlstra 2007; De Marco 2009; Miszalski et al. 2009b), there has never been a quantification of the link. The reason has been a lack of data. Binary modeling of known and newly discovered binary CSPNe along with spatiokinematic modeling of the PNe have shown that of the systems studied, all seem to show an alignment between the central binary axis and the primary geometrical axis of the PN. Including the two systems we provide values for in this paper, there are now eight known PNe with binary CSs for which both inclinations are known. Using these data, we are here, for the first time, demonstrating a correlation between post-CE CSs and their PN shapes, which we argue below implies causation.

2. OBSERVATIONS AND REDUCTIONS

2.1. Photometry

We utilize the orbit-resolved *B*, *V*, and *R* photometry from Hillwig et al. (2010) for the CS of NGC 6337. As described in Hillwig et al. (2010), the photometry shows clear and consistent, nearly sinusoidal, variability of nearly identical amplitudes in all three filters. The photometry is presented in differential magnitudes via single star differential photometry, with two additional comparison stars used to confirm that our first comparison star is not photometrically variable.

Photometric variability of the nucleus of Sp 1 was originally discovered in 1988 by H. E. Bond. It was chosen for photometric monitoring because Mendez et al. (1988) had

---

[9] Visiting astronomer, Cerro Tololo Inter-American Observatory, National Optical Astronomy Observatory, which is operated by the Association of Universities for Research in Astronomy, under contract with the National Science Foundation.

Table 1
Differential Magnitudes of the Central Star of NGC 6337

HJD (2450000+)	B_{diff} (mag)	σ_B (mag)	HJD (2450000+)	V_{diff} (mag)	σ_V (mag)	HJD (2450000+)	R_{diff} (mag)	σ_R (mag)
3477.79437	2.372	0.003	3477.79884	2.156	0.004	3477.80332	1.966	0.003
3477.80804	2.289	0.003	3477.81252	2.052	0.003	3477.81700	1.879	0.003
3477.82262	2.195	0.003	3477.82710	1.981	0.004	3477.83157	1.838	0.003

(This table is available in its entirety in machine-readable form.)

Table 2
Apparent Magnitudes of the Central Star of Sp 1

HJD (2400000+)	B (mag)	σ_B (mag)	HJD (2400000+)	V (mag)	σ_V (mag)	HJD (2400000+)	R (mag)	σ_R (mag)	HJD (2400000+)	I (mag)	σ_I (mag)
47223.7965	14.432	0.003	47223.8060	13.953	0.003	47223.8069	13.656	0.003	47223.8079	13.289	0.0040
47223.8008	14.436	0.003	47223.7977	13.948	0.003	47223.7988	13.650	0.003	47223.7998	13.291	0.0040
47223.8050	14.431	0.003	47223.8018	13.956	0.003	47223.8028	13.651	0.003	47223.8040	13.296	0.0040

(This table is available in its entirety in machine-readable form.)

reported an emission-line spectrum similar to that of the close binary central star of HFG 1, likely due to reprocessed radiation on the facing hemisphere of a companion. Observations in B, V, R, and I were made by H. E. Bond on the CTIO 0.9 m telescope during five observing runs in 1988–1990, and a preliminary photometric period of 2.91 days was reported in Bond & Livio (1990). The full data have not been published previously but are presented here.

Also included are new data from a number of telescopes: I-band data from the 0.6 m SARA telescope at CTIO (SARA-CT) in 2010 and 2011; V-, R-, and I-band photometry from the CTIO 0.9 m and 1.3 m telescopes in 2009; and more I-band data from the South African Astronomical Observatory in 2010.

The data show very consistent periodic behavior over the entire 23 year span of observations. However, there is a clear scatter around the nearly sinusoidal average that is larger than would be consistent with the uncertainties in the photometry. We discuss the implications and possible causes of this scatter below.

The apparent magnitudes for the CS of Sp 1 were calibrated using secondary standard stars in the Sp 1 field. Absolute photometry of the secondary standards was performed on a photometric night using Landolt standard stars (Landolt 1992).

Tables 1 and 2 give the differential and apparent magnitudes for the CSs of NGC 6337 and Sp 1, respectively (the full tables are given in the machine-readable versions).

2.2. Spectroscopy

We also obtained orbit-resolved spectroscopy for both CSs using the Gemini South telescope and the GMOS-S instrument in long-slit mode. The B1200 grating was used with a 0.75 arcsec wide slit with 2×2 binning and a central wavelength of 4750 Å, resulting in a wavelength range from 4000 to 5460 Å. The resolution of the B1200 grating is 3744, giving a $\Delta\lambda$ at our central wavelength of 1.27 Å. The resulting spectra have a pixel size in the spectral direction of 0.47 Å. We obtained ten pairs of 600 s exposures for NGC 6337 spread

over the orbital period and for Sp 1 we obtained 15 pairs of 480 s exposures.

The spectra of the CS of NGC 6337 (Figure 1) show clear emission lines due to an irradiated secondary as well as radial velocity variability with the photometric period. Also visible is broad hydrogen emission similar to those seen in HFG 1 (Exter et al. 2005) and Abell 65 (Hillwig et al. 2015). In this case as well, the broad H emission with narrow absorption core corresponds to the irradiated companion.

The spectra of the CS of Sp 1 (Figure 2) show emission lines from an irradiated cool companion as well as absorption lines of H and He II. Both sets of features vary in radial velocity with the photometric period.

All spectra were reduced with the GEMINI package in IRAF. Wavelength calibration was performed using CuAr arc spectra. Radial velocity values for each spectrum were found using line centers. For emission lines and weak absorption lines, line centers were found by Gaussian line fitting while for strong absorption features we used Voigt profile fitting. A resulting radial velocity for each spectrum used the average for a set of lines. The lines used for each system are described below. We also used cross-correlation fitting (CCF) to find radial velocities. The results from the two methods agreed to within uncertainties; however, because of the irradiation effect in both systems causing variations in line strength, the CCF results typically had larger uncertainties than simple centroid averaging of multiple lines.

For the initial visits to both targets, arc spectra were obtained at the beginning of the night rather than consecutively with the science spectra. In these spectra we found overall shifts of as much as 15 km s^{-1} in the average value of nebular line positions (which should remain stationary). Based on these results, all subsequent visits included arc spectra taken immediately before or after the science spectra. Using these arc spectra, the standard deviation of random spectral shifts between spectra were reduced to <2 km s^{-1} for the average positions of nebular lines.

Despite the average of all available nebular lines from one spectrum to another being consistent to within a few km s^{-1},
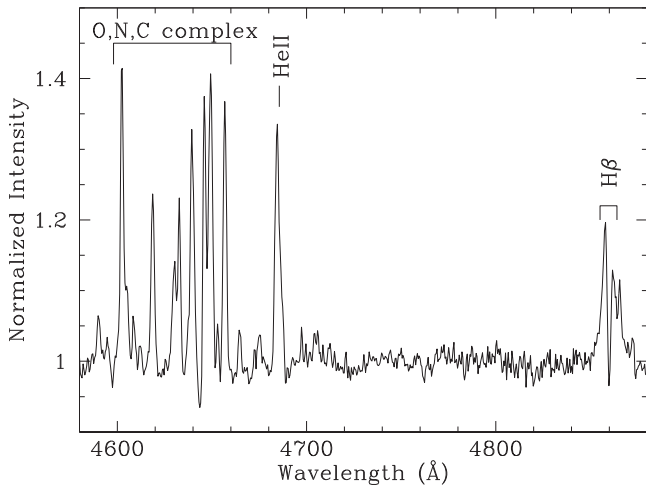
Figure 1. Example of the continuum normalized spectrum of the CS of NGC 6337 showing emission features from the irradiated secondary, including the broad Hβ feature.

Figure 2. Example of the continuum normalized spectrum of the CS of Sp 1 showing both emission features from the irradiated secondary and absorption features from the hot CS.

comparing *individual lines* for a given spectrum we find line-center differences of up to $15\,\mathrm{km\,s^{-1}}$, with a standard deviation of up to $5\,\mathrm{km\,s^{-1}}$. Given the spectral resolution and $\Delta\lambda$ of our spectra, these calibrations correspond to about one-tenth of a resolution element, which we find to be an acceptable calibration. However, the availability of the nebular lines allows us to *internally* calibrate each science spectrum. This includes the early spectra, which did not have arc spectra taken consecutively. We find an average and standard deviation for all spectral lines across all spectra (removing those with no consecutive arc spectra) for each system. We then use the difference of individual spectral lines in each spectrum from that average to create an internal wavelength calibration for the stellar spectra. Such an approach has been used successfully in the past (e.g., Jones et al. 2015).

For Sp 1 we find from the nebular lines a PN systemic velocity of $\gamma_{\mathrm{PN}} = -27 \pm 2\,\mathrm{km\,s^{-1}}$ and for NGC 6337 a PN systemic velocity of $-69 \pm 5\,\mathrm{km\,s^{-1}}$. We described these results in more context below.

For the CS and companion in Sp 1, the total radial velocity variation is only about $20\,\mathrm{km\,s^{-1}}$; the results were then very sensitive to the calibration variations mentioned above. However, in Figure 6 we show the double-lined radial velocity curve for the central binary in Sp 1, demonstrating that our final calibration is good enough to detect and measure the radial velocity variations of both components. The narrow emission lines provide the more precise curve of the two, while the broader absorption lines have correspondingly larger uncertainties and scatter. We find that the hydrogen absorption lines are not consistent throughout the orbit, often having what appears to be a blueshifted absorption component of the line, though the overall shape varies as well. We used multiple-component line fitting in an attempt to improve the radial velocity curve. However, we find that even with the improved fits, using only the hydrogen lines results essentially in a scatter plot in radial velocity. Thus the CS curve in Figure 6 uses only the He II absorption lines at $\lambda\lambda\,4541$, 4686, and 5411 Å.

For the CS of NGC 6337, we have only the emission lines and as mentioned, the radial velocity amplitude is much larger. Therefore, the resulting radial velocity curve of the cool companion in that system (Figure 3) has considerably better precision relative to amplitude.
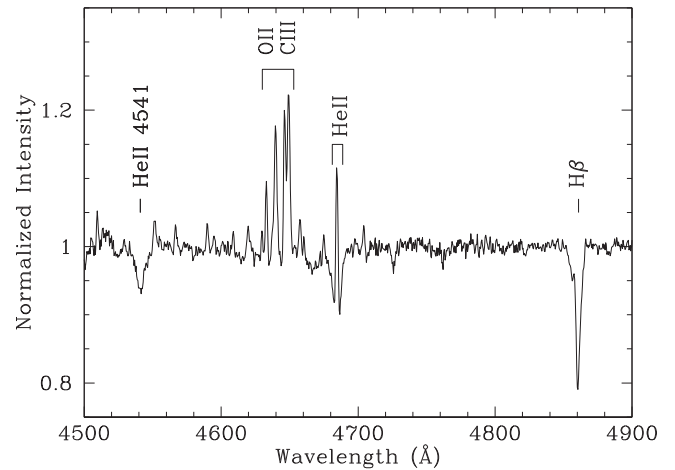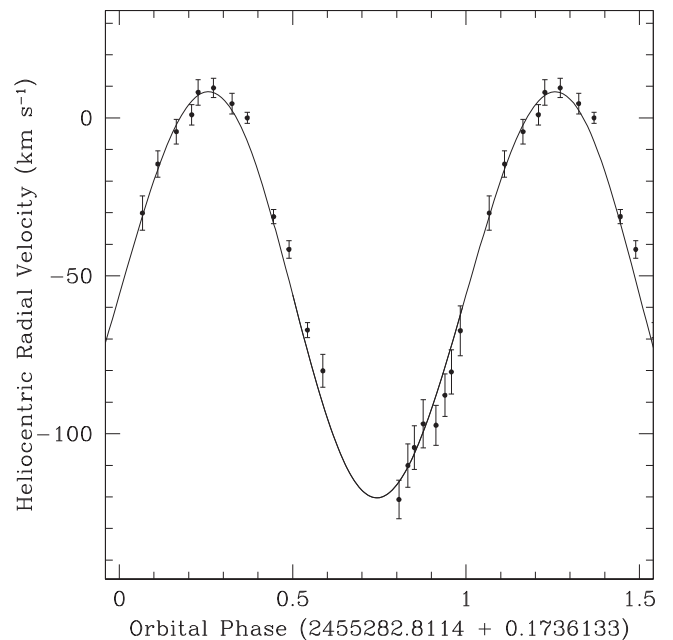

Figure 3. Phase-folded radial-velocity curve of NGC 6337 for the period given in the ephemeris (Equation (1)). The fit line is from the Wilson–Devinney model (Wilson & Devinney 1971; Wilson 1990) described in Section 3.2. We find a system velocity of $\gamma = -54 \pm 3\,\mathrm{km\,s^{-1}}$ with a radial-velocity amplitude for the secondary of $K_{\mathrm{CS}} = 63 \pm 2\,\mathrm{km\,s^{-1}}$.

3. NGC 6337

3.1. Overview

The CS of NGC 6337 was found by Hillwig (2004) to be a photometric variable consistent with a close binary system, with preliminary binary system modeling performed later (Hillwig et al. 2010). The reported period was 0.1734742 days although with some uncertainty due to possible aliasing. The range of possible models suggested a low to intermediate inclination binary system with a late M star companion and a CS that had nearly reached the WD cooling track. Weidmann et al. (2015) describe the emission-line spectrum of NGC 6337's CS, which is consistent with the finding that the system harbored an irradiated binary.

The radial velocity curve resulting from our data shows the variation of the emission lines from the heated secondary star (Figure 3), as described previously. The period of the radial velocity variations matches those of the photometric variations, confirming that this is indeed a binary system exhibiting an irradiation effect. However, the radial velocity data, combined with the photometry, provide a longer baseline, allowing us to improve the period determination. We find that the primary period reported in Hillwig et al. (2010) was in fact an alias period, one that was removed with the additional data. The true period is very close to the previously reported value. The improved ephemeris in HJD is

$$T = 2455282.8114(5) + 0.1736133(5)E. \qquad (1)$$

We use this improved period in our binary modeling, though in terms of the absolute physical parameters, the effect of the adjusted period is smaller than the uncertainties in the resulting parameters.

Nebular morphology modeling (García-Díaz et al. 2009) suggests a nebular inclination $\lesssim 10°$ based on the nearly circular appearance of the equatorial ring (thus nearly face-on) and low measured expansion velocities for the bright ring. The color image of NGC 6337 from Hillwig et al. (2010) is shown in Figure 7. We find from our images that the ring is not sharply delineated. Thus, assuming the equatorial ring is uniform in radius, inclinations as high as $\sim 20°$ still produce a nearly circular appearance. An inclination of $20°$ would only produce a 6% difference between the short and long axes of the projected ellipse. This corresponds to less than one-fifth of the width of the emission in the ring. In this case it would be difficult to detect such a small difference. Additionally, if the narrow waist is not thin but has some measurable vertical extent, as suggested by Corradi et al. (2000), then the axis ratios can become more complicated. In terms of the measured projected expansion velocities, a difference in inclination between $10°$ and $20°$ only results in a factor of two difference in the true expansion velocities. Given that the measured value quoted by García-Díaz et al. (2009) is uncertain to a factor of two, and that the ring shows internal motions up to $50 \, \mathrm{km \, s^{-1}}$ (Corradi et al. 2000), this range in inclinations does not seem improbable.

Our long-slit spectra, taken at a position angle (PA) of $90°$, provide radial velocities of the bright ring on either side of the CS. We find a difference of $\Delta V_r(\exp, \mathrm{PA} = 90) = 9.3 \pm 0.5 \, \mathrm{km \, s^{-1}}$ in the radial expansion velocities of the ring at this PA, giving a projected expansion velocity of $V_r(\exp, \mathrm{PA} = 90) \approx 4.6 \, \mathrm{km \, s^{-1}}$. Assuming the nebular symmetry axis has PA $\approx -45°$ from García-Díaz et al. (2009), and a tilted, symmetric ring or toroid, our measured value should be $\cos 45° = 0.707$ times the maximum radial expansion velocity of the ring measured at PA $= 45°$, giving $V_r(\exp, \mathrm{PA} = 45) \approx 6.5 \, \mathrm{km \, s^{-1}}$. If the ring is tilted by $20°$, the resulting deprojected expansion velocity would be about $19 \, \mathrm{km \, s^{-1}}$, which is consistent with the expected speed of slow winds and the expansion velocities of equatorial rings in these systems.

If we also look at the lower end of the inclination range for the NGC 6337 nebula, the faint but visible lobes shown by Corradi et al. (2000) and García-Díaz et al. (2009), showing what they identify as caps and jets, demonstrate that an inclination near zero is very unlikely. These features show point-symmetry around the central star with the caps and jets

located at slightly different PAs. Neither lobe shows much lateral extent from the $\approx 45°$ PA of the assumed major axis, suggesting that the lobes are not significantly wider than the bright ring. If we assume that the lobes and ring are cylindrical (have the same lateral extent from the symmetry axis), then using the angular extent of the lobes on the sky we can determine a relationship between the nebular inclination and the axial ratio (the height of the cylinder relative to the diameter or half-height, h, relative to the radius r of the nebula for small inclinations,

$$h/r = \frac{1}{\sin i}\left(\xi + \frac{\sin^2 i}{\cos i}\right) \approx \frac{\xi}{\sin i}$$

where ξ is the fractional extent of the lobes outside of the ring relative to the radius of the ring. From our CCD images of NGC 6337 we find a somewhat conservative value $\xi \approx 0.6$. In other words, the lobes appear to extend approximately 0.6 ring radii outside of the bright ring. Using this relationship for $i = 5°$ gives $h/r \approx 7$. Even for extreme nebulae, such as Hen 3-401, the axial ratio is around 5. For $i = 20°$ we find $h/r \approx 2$, which is a reasonable value for a young PN and perhaps nearing the lower expected limit for similar systems.

Based on these arguments we use a range of $5°$–$20°$ for the inclination of the PN.

System velocities from the literature fall very close to $-70 \, \mathrm{km \, s^{-1}}$ (Meatheringham et al. 1988; Corradi et al. 2000; García-Díaz et al. 2009). The average heliocentric velocity for our measurements of the ring at PA $= 90°$ is $-69 \pm 5 \, \mathrm{km \, s^{-1}}$, consistent with the previous values. However, our system velocity for the binary, determined from the radial velocity curve of the companion (Figure 3) is $\gamma = -54 \pm 3 \, \mathrm{km \, s^{-1}}$, which is measurably different than the nebular velocity. It is unclear why the binary system velocity seems to differ from the nebular velocity. There are several possible reasons including a triple system, some kind of kick to the binary system relative to the nebula, deceleration of the nebula due to interaction with the surrounding ISM, or a brightness center of the nebula that is offset from the geometric center (e.g., see the case of SuWt 2 in Jones et al. 2010a). We do not have clear evidence for any of these options so at present the reason remains unknown. Further discussion of possible causes of off-center CSPNe are given by Soker et al. (1998) and Soker (2015).

The previously published distances to NGC 6337 described in Hillwig et al. (2010) range from 0.86 to 1.7 kpc and are consistent with the recent mean value from Frew et al. (2016), $d = 1.45 \pm 0.43$ kpc. Frew et al. (2016) also give $E(B - V) = 0.60 \pm 0.14$, resulting in $A_V = 1.86$. We use the range in distance as a consistency check with our binary modeling, as described in Section 3.2.

3.2. NGC 6337: Modeling the Light and Radial-velocity Curves

Given our previous modeling (Hillwig et al. 2010), which we used as a starting point for this work, the addition of a single-lined radial velocity curve allowed us to provide much stronger limits on the possible system parameters. The amplitude of the companion's radial velocity curve was found to be $K_2 = 63 \pm 2 \, \mathrm{km \, s^{-1}}$. However, since this was found using the emission lines in the spectrum, it represents the amplitude of the center of light of the irradiated hemisphere rather than the center of mass of the star. Because the Wilson–Devinney

Table 3
Best-fit Model Physical Parameters for the CSs of NGC 6337 and Sp 1

Parameter	NGC 6337	Sp 1
M_{CS} ($M_\odot$)	0.56	0.52–0.60
M_2 ($M_\odot$)	0.14–0.35	0.52–0.90
T_{CS} ($\times 10^3$ K)	115 ± 5	80 ± 10
T_2 ($\times 10^3$ K)	4.5 ± 0.5	3.5–4.6
R_{CS} (Pole, $R_\odot$)	0.045–0.085	0.20–0.35
R_2 ($R_\odot$)	0.30–0.42	1.05–1.6
i (°)	17–23	7–11

code uses the center of light to produce its radial velocity points, and because we expect the irradiated hemisphere to dominate the light from the companion, the effect is corrected, at least to first order, in our modeling.

For our models we set the mass of the CS to be $M_{CS} = 0.56$ $M_\odot$ based on the value from Gorny et al. (1997). We discuss below the consistency of this value with our resulting parameter sets.

The results of our modeling are given in Table 3 and are shown as solid lines in Figures 3 and 4. The well-determined value for the companion's radial velocity amplitude (along with the set value for M_{CS}) provides a narrow range of system inclinations from our binary system modeling. If we allow the CS mass to vary slightly, then the inclination range expands with it; however, for a few tenths of a solar mass uncertainty in M_{CS} the inclination range expands by less than one degree. The resulting range of $17° \leqslant i \leqslant 23°$ overlaps with our adopted nebular inclination range. We also note that the model radial velocities are determined for the center of light, rather than the center of mass of the star. Since the radial velocity curve was determined from irradiation emission lines, and the irradiated hemisphere will dominate the light from the star, the model and data should be measuring the same thing.

Our parameter values for the secondary, M_2, R_2 and T_2, fall across roughly the same range as our previous results (Hillwig et al. 2010), with the range of possible companion masses, M_2, reaching slightly lower values. We have produced more precise results for the radius and temperature of the CS. We then find the resulting bolometric luminosity of the CS to be $467\,L_\odot$ $\lesssim L \lesssim 1100\,L_\odot$. Comparing these values for the CS with the post-AGB models of Schönberner (1983) we find that the results fall close to the evolutionary track of a $0.565\,M_\odot$ CS with an age between 20,000 and 24,000 years. Thus our assumption of the CS mass is consistent with our results.

Using VPHAS data (Drew et al. 2014) for the CS of NGC 6337 with $u = 14.908 \pm 0.004$, (MJD = 56566.00580) $u = 14.909 \pm 0.004$ (MJD = 56566.00805), $g = 16.206 \pm 0.003$ (MJD = 56566.01689), $g = 16.176 \pm 0.003$ (MJD = 56566.01931), r2 = 15.805 ± 0.004 (MJD = 56566.02531), and r2 = 15.800 ± 0.004 (MJD = 56566.02611) with VPHAS + filter profiles, we can interpolate to get $V = 16.00 \pm 0.04$ at MJD 56566.02, which corresponds to orbital phase 0.071 ± 0.001. Using our V-band light curve we then find a minimum light magnitude of 16.02 ± 0.04. Using this as the apparent magnitude, the interstellar absorption value described above, and our modeled parameters for the binary, we can calculate a distance to NGC 6337. In our models, we find that because of the low inclination, even at minimum light we are seeing a large portion of the irradiated hemisphere of the companion. Therefore, at minimum light the companion
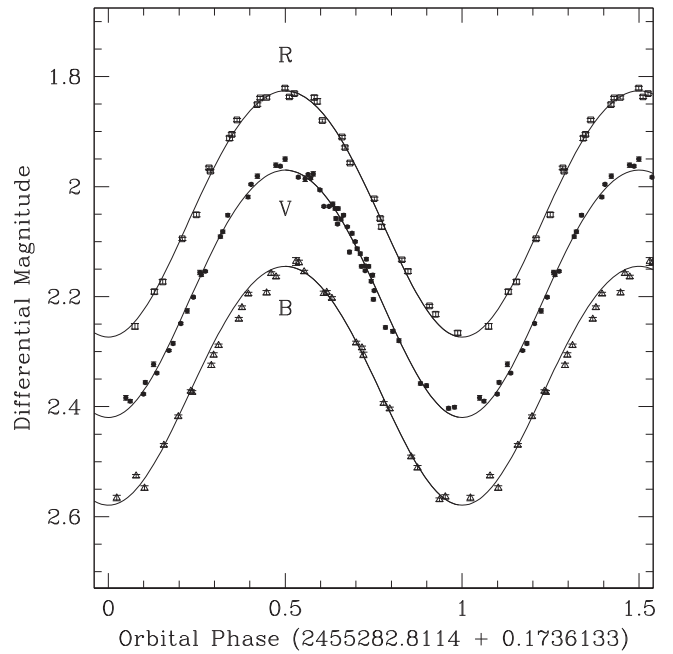

Figure 4. Phase-folded B-, V-, and R-band light curves of the CS of NGC 6337 for the period given in the ephemeris (Equation (1)). The curves have been vertically displaced from one another for clarity. The fit lines are from the Wilson–Devinney model discussed in Section 3.2.

contributes roughly 30% as much light as the CS in V. Using the total brightness at minimum light we find $d = 0.90$–1.3 kpc, which overlaps well with the distance estimates from the literature.

As with nearly all of the previous companion stars in these close binary systems, the companion here is overluminous compared to main sequence stars of equivalent mass. The radius in this case is similar to, or slightly larger than for an equivalent mass MS star, and the temperature is measurably higher.

4. SP 1

4.1. Overview

The PN Shapley 1 was discovered by Shapley (1936) who described it as a "fine ring" nebula with total diameter of 72 arcsec and width of the ring of 15 arcsec. Figure 7 shows a color composite image of Sp 1 using u, V, and R images. Sabbadin (1986) gives a distance for the PN of 1.5 kpc and Frew et al. (2016) give a mean statistical distance $d_{mean} = 1.46 \pm 0.43$ kpc using their surface brightness method, and an optically thin distance $d_{thin} = 1.19 \pm 0.24$ kpc. Frew et al. (2016) also give an interstellar reddening value $E(B - V) = 0.56 \pm 0.13$.

The CSPN of Sp 1 was discovered to be a periodic photometric variable, and likely binary, by Bond & Livio (1990), who give a period of 2.91 days. Because Sp 1 appears to be a nearly perfect circular ring, it was anticipated that the CS, if it were a binary, was seen nearly pole-on. In fact, the photometric amplitude was found to be small, about 0.1 mag in B (Bond & Livio 1990). The orbital period and photometric amplitude were confirmed by Bodman et al. (2012) who also published V, R, and I photometry as well, showing increasing amplitudes at redder wavelengths, as expected for a cool irradiated companion in such systems (De Marco et al. 2008).
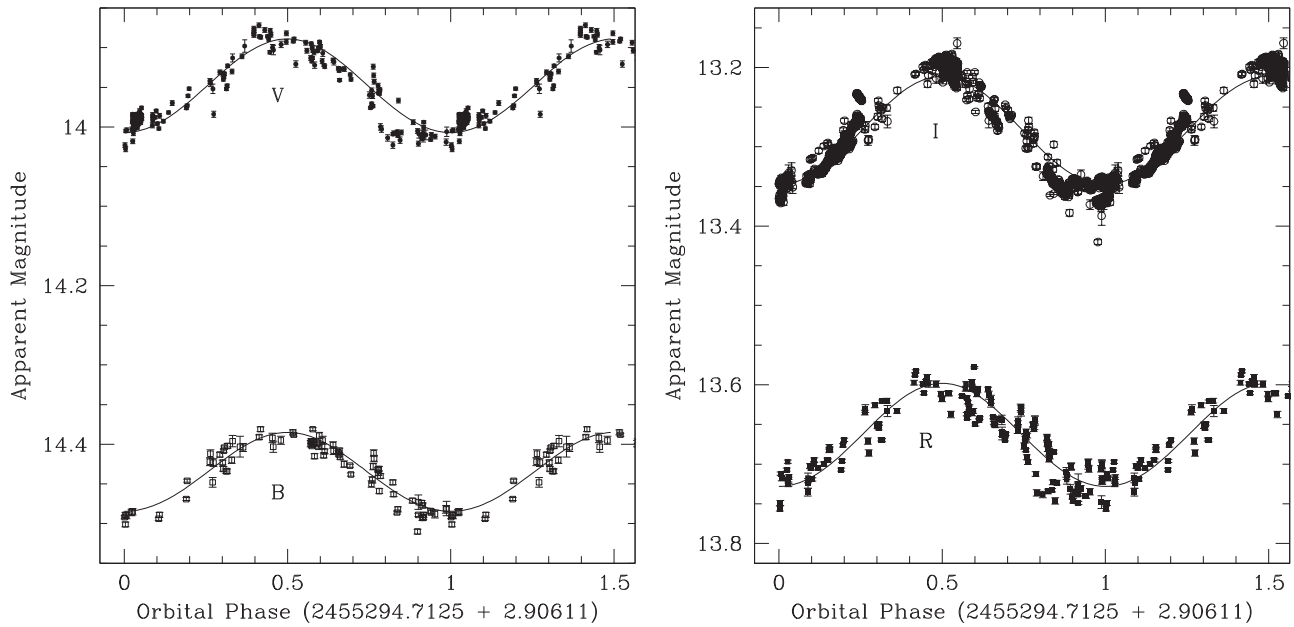
Figure 5. Phase-folded *B*, *V*, *R*, and *I* light curves for the CS of Sp 1 for the given ephemeris (Equation (2)). Also shown are the model light curves from the Wilson–Devinney code described in Section 4.2. No reddening correction has been applied.

Bodman et al. (2012) also performed preliminary binary modeling of the photometry using values from the literature for T_{CS}, R_{CS}, and M_{CS}. They also limited possible companions to MS stars. Even though most cool companions in short-period CSPN binaries are larger and hotter than their MS counterparts, this limitation allowed preliminary modeling with only light curves to produce converging parameter sets. Their resulting ranges for the physical parameters of the companion and the system inclination, based on their imposed modeling limits, were $1.16 \lesssim M_2 \lesssim 1.25$ $M_\odot$, $1.12 \lesssim R_2 \lesssim 1.20$ $R_\odot$, $5900 \lesssim T_2 \lesssim 6100$ K, and $15° \lesssim M_2 \lesssim 25°$ $M_\odot$. We compare our results, using fewer initial assumptions and including radial velocity curves, with theirs in Section 4.2.

Spatiokinematic modeling of the nebula was performed by Jones et al. (2012), who showed that the nebula appears to be nearly face-on with two small bright lobes and a slightly pinched waist. Their resulting inclination range was $i \approx 10°$–$15°$ for the nebula. They use $d = 1.5$ kpc from Sabbadin (1986) to determine a nebular age of ~8700 years. Their value is in agreement with that from Stasińska et al. (1997) who give an evolutionary time for the CS of 7400 years along with $M_{CS} = 5.87$ $M_\odot$. So Sp 1 appears to be roughly one-third the age of NGC 6337.

Jones et al. (2012) also describe photometric results demonstrating smooth variability with no sign of fast scatter due to mass transfer.

Using the photometry described in Section 2.1 (Figure 5) along with the radial velocity curve described in Section 2.2 (Figure 6), we find an updated orbital period in HJD of

$$T = 2455294.7125(2) + 2.90611(3)E \qquad (2)$$

for the binary CS of Sp 1. As mentioned in Section 2.1 the period is consistent over the entire 23 year span of data. However, the scatter about the sinusoidal irradiation effect is clearly larger than would be expected based on the photometric errors. Our results are consistent with the observation of Jones et al. (2012), showing no evidence of fast "flickering" that may
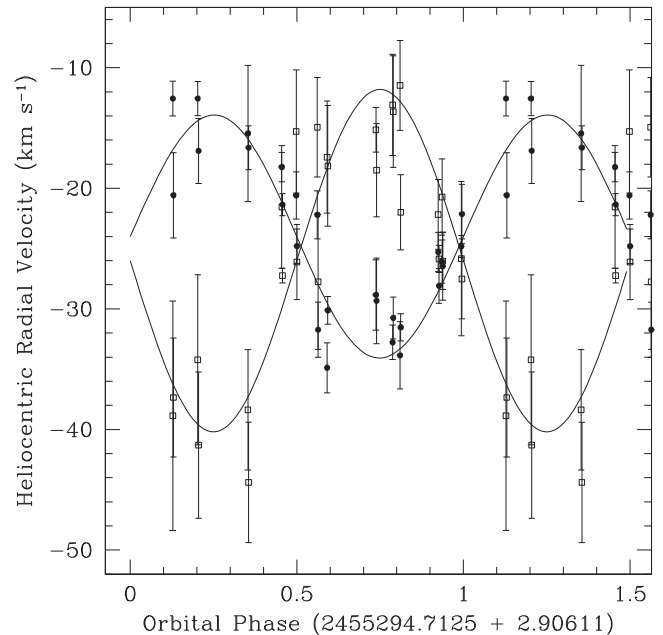

Figure 6. Phase-folded radial-velocity curve of the CS (hollow squares) and cool companion (*solid circles*) in Sp 1 for the period given in the ephemeris (Equation (2)). The fit lines are from the Wilson–Devinney model described in Section 4.2. We find a system velocity of $\gamma = -24$ km s^{-1} with a radial-velocity amplitude for the cool companion of $K_2 = 9.2 \pm 0.8$ km s^{-1} and for the CS of $K_2 = 13 \pm 2$ km s^{-1}.

be associated with mass transfer or even an accretion disk in the system. The scatter appears to be based on relatively slow variations in brightness. In order to explore this more, we removed the irradiation variability by subtracting our resulting binary model (described below in Section 4.2) from the light curves and performing a period search on the resulting difference light curve using the *Period04* software. For the entire sample we find no consistent periodicity. However, for data obtained over relatively short times we find several

potential periodicities showing nearly sinusoidal variability. Unfortunately, there is significant aliasing due to data sampling and none of the potential periods are consistent from one epoch of data to another. At this point we are unable to determine the source of the scatter or if it is periodic in nature.

We note that in several filters the data appear too faint around phase 0.8–0.9, most notably the V and I bands. It is possible that this is a systematic trend in the light curve, potentially due to heat transfer away from the substellar point. However, the effect is less noticeable in the B and R light curves. Most notably, the data in V and I at phase 0.8 were taken on the same nights (along with some R data) in 2009. However, no B data were taken at that time. Additional R data taken in 2009 on different nights add significant scatter at these phases, some of which are brighter than the model. It is possible that the faint appearance near phase 0.8–0.9 is simply due to a predominance of data taken on only a few nights at a time when the system was in the fainter state of its slow brightness variations (non-irradiation related).

4.2. Sp 1: Modeling the Light and Radial-velocity Curves

Having light curves in four filters, along with radial velocity amplitudes for both stars in the binary system, has allowed us to determine the physical parameter values for the binary system with relatively tight constraints. Inspecting the spectra we find that no He I lines are visible, meaning a temperature of >70 kK. We find that a temperature of 80 kK matches the He II absorption lines relatively well, although with emission from the nebula and irradiation lines from the companion filling in the lines, it is difficult to match them precisely. However, the line wings suggest a $\log g$ value between 5.0 and 5.5.

For the purposes of our binary modeling we use $T_{CS} = 80$ kK and try to maintain a $\log g$ value in the range suggested above. Using these two values and the mass determined by Stasińska et al. (1997) of $M_{CS} = 0.587 \ M_\odot$ we find a luminosity that roughly agrees with post-AGB models for stars of that mass and luminosity.

From the irradiation lines in the spectrum we find a projected orbital velocity relative to the center of mass for the cool companion of $K_2 = 9.2 \pm 0.8$ km s^{-1} and a zero-point velocity of $\gamma = -24 \pm 2$ km s^{-1}. This is in agreement with the heliocentric systemic velocity of the nebula determined from the nebular lines, which we find to be $\gamma_{PN} = -27 \pm 2$ km s^{-1}. Our values also agree with the value from Meatheringham et al. (1988) of $\gamma_{PN} = -31 \pm 3$ km s^{-1} but do not agree well with that of Jones et al. (2012) who find $\gamma_{PN} = -18 \pm 5$ km s^{-1}.

The radial velocity amplitude of the CS determined from the He II absorption lines is found to be $K_{CS} = 13 \pm 2$ km s^{-1} with a zero-point velocity of $\gamma = -27 \pm 4$ km s^{-1}. We use the radial velocity amplitude values to restrict the system mass ratio in our modeling. However, because the irradiation lines trace the irradiated hemisphere rather than the center of mass, the velocity amplitude for the companion is likely larger than the value quoted above. Using the Wilson–Devinney code, and taking the resulting curve from those models, based on the center of light of the star, we find that the center of mass velocity is approximately 2 km s^{-1} greater in amplitude than the center of light curve. We then adopt $K_2 = 11.2 \pm 0.8$ km s^{-1} and $K_{CS} = 13 \pm 2$ km s^{-1}. From these we find the system mass ratio to be $q = 1.2 \pm 0.2$.

Even though the system is not eclipsing, the information we obtain from the radial velocity data combined with the

irradiation effect amplitudes limit the system inclination to the range $7° \lesssim i \lesssim 11°$. The remainder of the parameter ranges from the modeling is given in Table 3.

The resulting parameters for the companion show a star too big for an MS equivalent of that mass, as we typically see in these systems. However, the temperature, which is typically higher in close binary CSPN companions, is lower in this case for most of the parameter combinations. For the lower end of companion masses, the stellar temperature is slightly above that expected for an MS star of that mass. At these masses though the radius is approaching twice the MS value. So either the companion is too cool compared to what we would expect, or it is significantly larger than expected, even for an irradiated companion.

The resulting $\log g$ range for the CS is slightly smaller in the model results relative to that from the spectrum. We find a most likely range for the CS mass in a range typical of CSPNe. We compared the CS values with post-AGB evolutionary models from Schönberner (1983) and found that over most of the range our masses from modeling are consistent with those results and give a very rough age range consistent with the dynamical age of Jones et al. (2012). However, the lower end of the CS mass range in our models produces ages inconsistent with the dynamical age of the nebula. If we require the CS to match the dynamical age of the PN, we find $M_{CS} \gtrsim 0.55 \ M_\odot$.

The binary parameters also allow us to calculate a distance to the nebula. The total intrinsic system brightness for the models used with the minimum apparent magnitudes from our light curves give a nebular distance in the range 1.0–1.5 kpc, which is again consistent with published values, especially those of Frew et al. (2016).

The differences between our results and those of Bodman et al. (2012) are due to the addition of the radial velocity data, which limits the results to the lower end of their inclination range. Also allowing our models to have companions with radii and temperatures that did not match their MS counterparts allowed fits to the light curves at lower inclinations, which were also consistent with the radial velocity data.

5. INCLINATIONS OF KNOWN PNe WITH BINARY CENTRAL STARS

In the current published literature we find eight PNe with close binary CSs for which an inclination has been determined for both the nebula and the central binary. Those eight are Abell 63 (Bell et al. 1994; Mitchell et al. 2007; Afşar & Ibanoğlu 2008), Hartl-Triton 4 (Tyndall et al. 2012; Hillwig et al. 2016), NGC 6778 (Miszalski et al. 2011; Guerrero & Miranda 2012), Abell 41 (Bruch et al. 2001; Shimanskii et al. 2008; Jones et al. 2010b), Abell 65 (Huckvale et al. 2013; Hillwig et al. 2015), Henize 2–428 (Rodríguez et al. 2001; Santander-García et al. 2015), and the two presented here, NGC 6337 (García-Díaz et al. 2009) and Sp 1 (Jones et al. 2012).

In Figure 7 we show images of each of these nebulae (not to the same scale). Images are from left to right: (top row) Abell 63 (Corradi et al. 2015), HaTr 4 (ESO NTT archive), NGC 6778 (Guerrero & Miranda 2012), Abell 41 (Jones et al. 2010b), (bottom row) Abell 65 (Huckvale et al. 2013), Hen 2-428 (Santander-García et al. 2015), NGC 6337 (Hillwig et al. 2010), and Sp 1 (our image).

In every case, the inclinations of the PN and central binary are consistent with one another, where *inclination* for the PN is
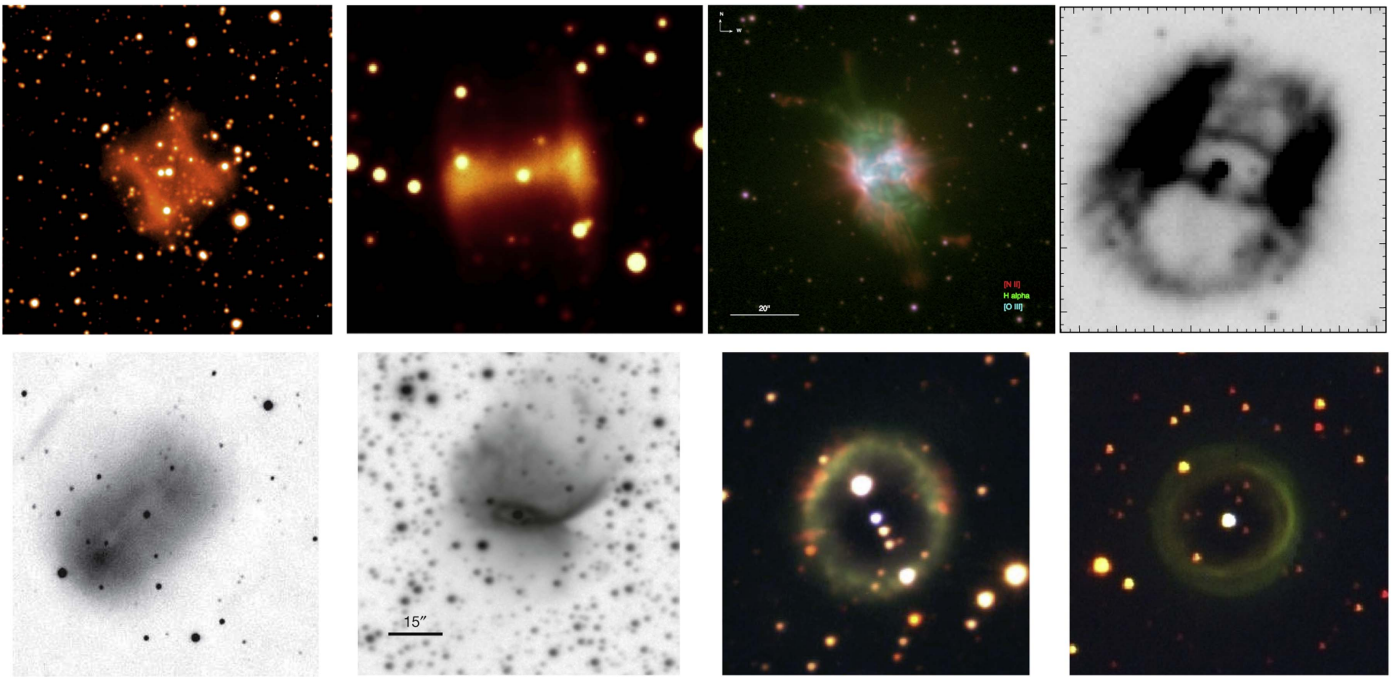
Figure 7. Images of each of the eight PNe for which both nebular inclination and binary inclination for the close binary CSs have been published. Top row: Abell 63, HaTr 4, NGC 6778, and Abell 41. Bottom row: Abell 65, Hen 2-428, NGC 6337, and Sp 1. See the text for details.

defined as the inclination of the primary axis of symmetry relative to the line of sight and for the binary it is the inclination of the orbital axis relative to the line of sight (as is typical for binary-star analyses). Therefore, agreement between the two inclinations means that, within the uncertainties, *the binary orbital axis is aligned with the nebular symmetry axis*. HaTr 4 is the only case in which the binary and nebular inclination ranges do not overlap, though they do meet at the extreme and the binary inclination is based on modeling of the light curves only and is thus a relatively uncertain range.

There is one potential example of a wide binary CSPN for which the binary and nebular axes do not align, the case of LoTr 5. Van Winckel et al. (2014) show that in order for the wide binary axis to align with the published value for the nebular axis of $17°$ (Graham et al. 2004), the hot CS would need to have a close companion with a mass of several solar masses. However, there is currently no clear evidence for such a close companion. This may then be a case of misalignment between the binary and nebula. The binary period is not known but is at least on the order of several thousand days, meaning this system likely avoided the CE phase and is thus not analogous to the close-binary, post-CE systems.

We show in Figure 8 the inclinations for each of the eight systems described above plotted against one another. The solid line has a slope of one, showing where each data point would fall if the binary and PN are aligned. The error bars for the nebular inclinations are approximate values in those cases where the published description did not give a range or error bars. The binary inclination error bars are those quoted in the corresponding papers.

We have plotted the assumed value in the middle of the quoted range except for NGC 6778, for which Miszalski et al. (2011) show the CS to be an eclipsing binary. While no binary modeling has been published for this object (we are pursuing formal modeling of the light curves and have recently obtained orbit-resolved spectroscopy to measure radial velocity values),
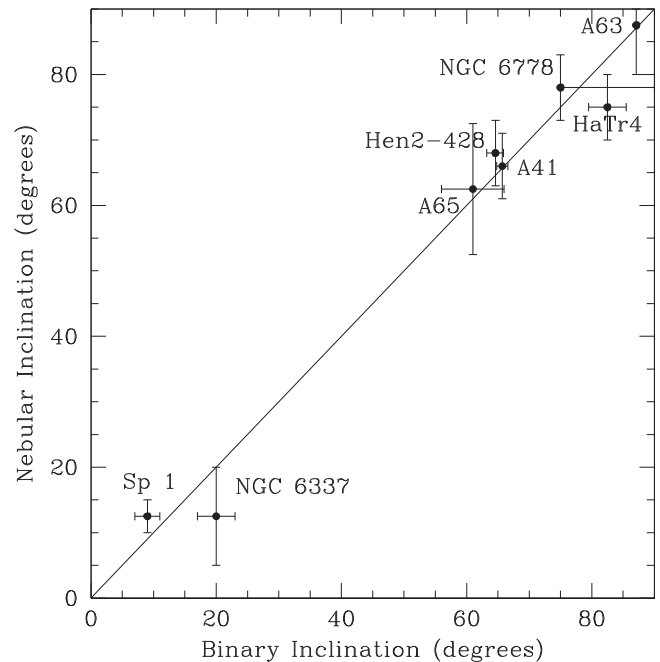

Figure 8. Nebular and binary system inclinations for PNe with known binary CSs. This represents all of the systems for which these values have been modeled. See the text for details.

we take $75°$ to be an approximate lower limit to the binary inclination in order to see eclipses. The light curve clearly shows partial eclipses, so it is unlikely that the binary inclination is approaching $90°$, but without further data we leave the top end of the range open.

While it may be tempting to perform a χ^2 test on the data plotted in Figure 8 in order to statistically explore the correlation between binary and nebular inclinations, there is an additional parameter not shown in the figure. Like radial

Table 4
Inclination Ranges from the Literature and Probabilities of Agreement

PN Name	i_{bin} (deg)	$(\cos i_1 - \cos i_2)$ (binary)	i_{neb} (deg)	$(\cos i_1 - \cos i_2)$ (nebula)	$\sum P$
Abell 63	86.9–87.3	0.0070	80–90	0.1736	0.1806
HaTr 4	80–85	0.1038	70–80	0.2549	0.3586
NGC 6778	75–90	0.2588	73–83	0.1705	0.4293
Abell 41	64.8–66.6	0.0286	61–71	0.1592	0.1879
Abell 65	56–66	0.1525	52–72	0.3066	0.4591
Hen 2-428	63.2–65.9	0.0425	63–73	0.1616	0.2042
NGC 6337	17–23	0.0358	5–20	0.0565	0.0792
Sp 1	7–11	0.0109	10–15	0.0189	0.0298

Note. Column 2 gives the binary system inclination from modeling, column 3 shows the fractional surface area on a sphere covered by the binary inclination range, columns 4 and 5 give the same values but for the PN, and column 5 gives the sum of the two fractional solid angles.

velocity, inclination does not tell us the three-dimensional alignment of the axis. It is a projection of the alignment onto the line of sight. In each case we must also consider the PA of the axes. We can typically determine the PA of each PN from images and spectroscopy, but these values are not known for the central binaries. Thus the binary orbit may, or may not, be aligned with the nebula. Statistically, a binary with inclination near 90° but with unknown PA still has a large uncertainty in the three-dimensional orientation of its orbital axis. However, because the binary inclinations for the CSs of Sp 1 and NGC 6337 are low, the PAs have a much smaller effect on the possible range in physical orientation of their orbital axes.

To consider the physical alignment of a binary system, we take a sphere centered on the binary. The inclination angle points to some point on the sphere. We can then rotate the system 360° in PA about our line of sight. The area swept out on the sphere, given the uncertainty in the inclination, during that rotation describes the possible orientations of the axis. That surface area on the sphere relative to the area of a half-sphere (since we do not discriminate between the two poles of the orbit) gives the fractional area covered by the possible orbital orientation. Thus for equivalent uncertainties, a binary with low inclination, pointing close to along the line of sight, will produce a much smaller fractional surface area.

If we determine the surface area on the same sphere for the nebular inclination, then we can compare the two not only to see if they overlap, but also to determine the probability that they would overlap if the two axial orientations were random and had no physical connection. For random orientations, taking the sum of the two fractional areas gives the maximum probability that they will overlap randomly. For our purposes here we ignore the PA measurements of the nebulae, thus giving an upper limit to the probabilities. However, as we show below, even the upper limit we find is convincing in terms of a physical relationship between PN shaping and the central binary.

The surface area on the sphere for a given inclination range from i_1 to i_2 and with no PA value ($\int d\phi = 2\pi$) is given by

$$\int_{i_1}^{i_2} 2\pi r^2 \sin i \, di = -2\pi r^2 \cos i \big|_{i_1}^{i_2}.$$

With the surface area of a half-sphere equal to $2\pi r^2$ then the fractional area is just $(\cos i_1 - \cos i_2)$.

Applying this equation to the inclination ranges published for the binary and nebular inclinations gives us the results shown in Table 4. Column 6 in the table gives the sum of the

fractional areas, $\sum P$, which is the probability of a chance alignment of the PN and central binary. The probabilities for NGC 6337 and Sp 1 are roughly 8% and 3%, respectively.

While the individual probabilities of chance alignment are low for a number of these systems, the real significance at this point is in the number of systems that we now have. The probability that *all* of these systems would be aligned by chance is the product of the individual probabilities. Taking the product of the $\sum P$ values from Table 4 we find a 0.00009% likelihood of random alignment of *all* of these systems.

Does this require that the shape of the nebula be caused by the central binary? No, not from this information alone. These results demonstrate a very high correlation between the close binary and PN axes. For example, it is possible that the individual stellar rotations are in the same plane as the binary orbit. In that event, the stellar rotation axes would also be aligned with the nebular axes and may have determined the nebular orientation. It is possible that some large-scale effect, such as local or even galactic magnetic fields, determined the orientation of the binary when it formed *and* produced the shape of the binary (for a discussion of PNe and Galactic B-fields, see Rees & Zijlstra 2013).

However, given recent work demonstrating the difficulty of having stellar rotation produce shaping, and the potential ability of binary systems to produce the observed shapes (nor07), we believe that our results provide overwhelming observational evidence for a physical link between close binary CSPNe and the physical structure of their surrounding nebula.

6. DISCUSSION AND CONCLUSION

We have shown conclusively that the CSs of both NGC 6337 and Sp 1 are short-period irradiated binary systems with cool companions in low inclination orbits. The companions in both systems appear to be larger than a main sequence counterpart of the same mass, as is typical in these systems. The companions are also typically hotter than expected for a main sequence counterpart. However, we find that in the case of Sp 1 the companion may be roughly the same temperature, or cooler. It is unclear why this is the case here. The secondary *may* be slightly evolved, though there is no evidence to support this possibility. The companion in NGC 6337 does show a typically higher temperature.

The modeled inclinations of both binary systems also align with the inclinations of the surrounding nebulae. We show that these two systems, now along with six other systems, make a sample of eight PNe for which the nebular inclination and

binary inclination of a close binary CS are known. In all eight cases the two inclinations agree with one another, within the uncertainties. We demonstrate that the likelihood that all eight of these systems are aligned merely by chance is vanishingly small. All other known parameters considered, the conclusion of a causal link between binarity and the axial symmetry of the PN is now on solid statistical grounds.

Post-CE PNe have already been tentatively associated with bipolar morphologies (Zijlstra 2007; De Marco 2009; Miszalski et al. 2009b) although the link is not clear cut because some of the PNe do not show the distinctive bi-lobal structure (e.g., M2-29; Hajduk et al. 2008). From CE simulations (e.g., Sandquist et al. 1998; Passy et al. 2012) it is clear that the ejection of the CE happens preferentially on the equatorial plane. This equatorial ejection is a torus with a very large scale height. The scale height is likely a function of the companion mass because it depends on the amount of angular momentum injected, which is larger for a more massive companion. A more massive companion also induces a stronger tide on the giant, which in turn results in more distant companions being captured into a CE interaction by the AGB star. These more massive and more distant companions carry more angular momentum into the envelope at the time of in-spiral.

Magnetic fields in CE interactions likely play an important dynamical role in the ejection (e.g., Regős & Tout 1995), and can be investigated by jets observed in PNe. Some post-CE PNe have jets. Jet masses and kinematics have been measured (e.g., Jones et al. 2014) and exploited to determine the likely magnetic field strength and geometry at the time of CE (Tocknell et al. 2014). They also allow us to determine the elusive timescales of CE events, such as the length of the pre-in-spiral phase or the formation of post-CE accretion disks after the in-spiral by a new phase of Roche lobe overflow or fall-back of envelope gas (Kuruwita et al. 2016).

Once the in-spiral takes place, it is over very quickly (of the order of a dynamical timescale of the giant, which is between a month and a year for the giants of interest here). On the assumption that the envelope is actually ejected during the dynamical in-fall (something that is currently debated; Nandez et al. 2015; Iaconi et al. 2016), we can assume that the orbital separation of the post-in-spiral giant is approximately the same as we see today. This means that the giant star is quickly changed to a star with a radius smaller than today's Roche lobe radius. Since the luminosity is fully dependent on the core mass, it does not change. As a result the temperature of the CS must incur a relatively similar increase. The least massive companions would, at least, in principle sink deeper into the envelope of the giant to eject it. This may generate a correlation between orbital separations and companion mass, although one may have to account for more massive primaries likely needing more orbital shrinkage to eject the massive envelope. In conclusion, a number of complex correlations are expected among stellar, binary and PN parameters in these objects, something that we will be able to test thanks to continuous characterization of these objects increasing the number of accurate parameters available. Soon PNe will become the best testing ground of the CE interaction.

But for now, we have demonstrated observationally a statistically significant connection between close binary CSs and their surrounding PN.

REFERENCES

Afşar, M., & Ibanoğlu, C. 2008, MNRAS, 391, 802

Bell, S. A., Pollacco, D. L., & Hilditch, R. W. 1994, MNRAS, 270, 449

Bodman, E. H. L., Schaub, S. C., & Hillwig, T. 2012, JSARA, 5, 19

Bond, H. E. 2000, in ASP Conf. Ser. 199, Asymmetrical Planetary Nebulae II: From Origins to Microstructures, ed. J. H. Kastner, N. Soker, & S. A. Rappaport (San Francisco, CA: ASP), 115

Bond, H. E., & Livio, M. 1990, ApJ, 355, 568

Bruch, A., Vaz, L. P. R., & Diaz, M. P. 2001, A&A, 377, 898

Corradi, R. L. M., García-Rojas, J., Jones, D., & Rodríguez-Gil, P. 2015, ApJ, 803, 99

Corradi, R. L. M., Goncalves, D. R., Villaver, E., et al. 2000, ApJ, 535, 823

De Marco, O. 2009, PASP, 121, 316

De Marco, O., Hillwig, T., & Smith, A. J. 2008, AJ, 136, 323

De Marco, O., Long, J., Jacoby, G. H., et al. 2015, MNRAS, 448, 3587

Drew, J. E., Gonzalez-Solares, E., Greimel, R., et al. 2014, MNRAS, 440, 2036

Exter, K. M., Pollacco, D. L., Maxted, P. F. L., Napiwotzki, R., & Bell, S. A. 2005, MNRAS, 359, 315

Frew, D. J., Parker, Q. A., & Bojičić, I. S. 2016, MNRAS, 455, 1459

García-Díaz, Ma. T., Clark, D. M., López, J. A., Steffen, W., & Richer, M. G. 2009, ApJ, 699, 1633

Gorny, S. K., Stasinska, G., & Tylenda, R. 1997, A&A, 318, 256

Graham, M. F., Meaburn, J., López, J. A., Harman, D. J., & Holloway, A. J. 2004, MNRAS, 347, 1370

Guerrero, M. A., & Miranda, L. F. 2012, A&A, 539, A47

Hajduk, M., Zijlstra, A. A., & Gesicki, K. 2008, A&A, 490, L7

Hillwig, T. C. 2004, in ASP Conf. Ser. 313, Asymmetrical Planetary Nebulae III: Winds, Structure and the Thunderbird, ed. M. Meixner et al. (San Francisco, CA: ASP), 529

Hillwig, T. C., Bond, H. E., Afşar, M., & De Marco, O. 2010, AJ, 140, 319

Hillwig, T. C., Bond, H. E., Frew, D. J., Schaub, S. C., & Bodman, E. H. L. 2016, AJ, 152, 34

Hillwig, T. C., Frew, D. J., Louie, M., et al. 2015, AJ, 150, 30

Huckvale, L., Prouse, B., Jones, D., et al. 2013, MNRAS, 434, 1505

Iaconi, R., Reichardt, T., Staff, J., et al. 2016, MNRAS, 464, 4028

Ivanova, N., Justham, S., Chen, X., et al. 2013, A&ARv, 21, 59

Jones, D., Boffin, H. M. J., Rodríguez-Gil, P., et al. 2015, A&A, 580, A19

Jones, D., Lloyd, M., Mitchell, D. L., et al. 2010a, MNRAS, 401, 405

Jones, D., Lloyd, M., Santander-Garcícõa, M., et al. 2010b, MNRAS, 408, 2312

Jones, D., Mitchell, D. L., Lloyd, M., et al. 2012, MNRAS, 420, 2271

Jones, D., Santander-Garcia, M., Boffin, H. M. J., Miszalski, B., & Corradi, R. L. M. 2014, in Asymmetrical Planetary Nebulae VI, ed. C. Morisset, G. Delgado-Inglada, & S. Torres-Peimbert (Mexico City: Universidad Nacional Autonoma de Mexico), 43, http://www.astroscu.unam.mx/apn6/PROCEEDINGS/

Kuruwita, R. L., Staff, J., & De Marco, O. 2016, MNRAS, 461, 486

Kwitter, K. B., Méndez, R. H., Peña, M., et al. 2014, RMxAA, 50, 203

Landolt, A. U. 1992, AJ, 104, 340

Meatheringham, S. J., Wood, P. R., & Faulkner, D. J. 1988, ApJ, 334, 862

Mendez, R. H., Kudritzki, R. P., Herrero, A., Husfeld, D., & Groth, H. G. 1988, A&A, 190, 113

Miszalski, B., Acker, A., Moffat, A. F. J., Parker, Q. A., & Udalski, A. 2009a, A&A, 496, 813

Miszalski, B., Acker, A., Parker, Q. A., & Moffat, A. F. J. 2009b, A&A, 505, 249
Miszalski, B., Jones, D., Rodríguez-Gil, P., et al. 2011, A&A, 531, A158
Mitchell, D. L., Pollacco, D., O'Brien, T. J., et al. 2007, MNRAS, 374, 1404
Morris, M. 1981, ApJ, 249, 572
Nandez, J. L. A., Ivanova, N., & Lombardi, J. C. 2015, MNRAS, 450, L39
Nordhaus, J., Blackman, E. G., & Frank, A. 2007, MNRAS, 376, 599
Passy, J.-C., Mac Low, M.-M., & De Marco, O. 2012, ApJL, 759, L30
Rees, B., & Zijlstra, A. A. 2013, MNRAS, 435, 975
Regős, E., & Tout, C. A. 1995, MNRAS, 273, 146
Rodríguez, M., Corradi, R. L. M., & Mampaso, A. 2001, A&A, 377, 1042
Sabbadin, F. 1986, A&AS, 64, 579
Sandquist, E. L., Taam, R. E., Chen, X., Bodenheimer, P., & Burkert, A. 1998, ApJ, 500, 909
Santander-García, M., Rodríguez-Gil, P., Corradi, R. L. M., et al. 2015, Natur, 519, 63

Schönberner, D. 1983, ApJ, 272, 708
Shapley, H. 1936, BHarO, 902, 26
Shimanskii, V. V., Borisov, N. V., Sakhibullin, N. A., & Sheveleva, D. V. 2008, ARep, 52, 479
Soker, N. 2015, ApJ, 800, 114
Soker, N., Rappaport, S., & Harpaz, A. 1998, ApJ, 496, 842
Stasińska, G., Gorny, S. K., & Tylenda, R. 1997, A&A, 327, 736
Tocknell, J., De Marco, O., & Wardle, M. 2014, MNRAS, 439, 2014
Tyndall, A. A., Jones, D., Lloyd, M., O'Brien, T. J., & Pollacco, D. 2012, MNRAS, 422, 1804
Van Winckel, H., Jorissen, A., Exter, K., et al. 2014, A&A, 563, L10
Weidmann, W. A., Méndez, R. H., & Gamen, R. 2015, A&A, 579, A86
Wilson, R. E. 1990, ApJ, 356, 613
Wilson, R. E., & Devinney, E. J. 1971, ApJ, 166, 605
Zijlstra, A. A. 2007, BaltA, 16, 79